# Nonuniform Sampling Pattern Design for Compressed Spectrum Sensing in Mobile Cognitive Radio Networks

Zihang Song, *Member, IEEE*, Yiyuan She, *Senior Member, IEEE*, Jian Yang, *Member, IEEE*, Jinbo Peng, *Student Member, IEEE*, Yue Gao, *Fellow, IEEE*, and Rahim Tafazolli, *Senior Member, IEEE*

***Abstract*—Compressed spectrum sensing (CSS) plays a pivotal role in dynamic spectrum access within mobile cognitive radio networks by offering reduced power consumption and lower hardware costs. The multicoset sampler, a well-known implementation for periodic nonuniform sampling, has been widely studied and is considered a promising architecture for realizing CSS. This article focuses on the design of the multicoset sampling pattern, aiming at enhancing the isometry property of the sensing matrix. Unlike previous studies which assume a noise-free setup, our work considers the problem in a real-world environment with noise. First, we propose a deterministic algorithm for sampling pattern generation, particularly for specific hardware setup parameters. This algorithm offers strict mutual-coherence control in the multicoset sensing matrix. To address more general hardware configurations, we propose two optimization algorithms. One of them searches for nearly optimal sampling patterns through a random search strategy, while the other employs a greedy pursuit strategy to find a local optimizer. Furthermore, we propose an algorithm to iteratively optimize the sampling pattern between consecutive spectrum sensing windows by minimizing a restricted version of mutual coherence. The excellent performance of our proposed algorithms has been demonstrated through numerical experiments and has been verified on a self-developed hardware platform.**

***Index Terms*—Compressed spectrum sensing, dynamic spectrum access, sensing matrix design, noise-robust algorithms.**

## I. Introduction

THE dynamic spectrum access (DSA) technique enables unlicensed secondary users (SUs) to efficiently utilize spectrum holes, thereby alleviating spectrum scarcity [1]. In cognitive radio (CR) networks, DSA primarily relies on spectrum sensing, a critical operation that empowers SUs to faithfully locate spectrum holes. With the commercialization of 5G and the emergence of 6G, CR devices are increasingly challenged to sense a broader multi-gigahertz spectrum. This expansion places higher demands on the speed of analog-to-digital converters (ADCs) and digital signal processors (DSPs), thereby exacerbating the power consumption and cost burden.

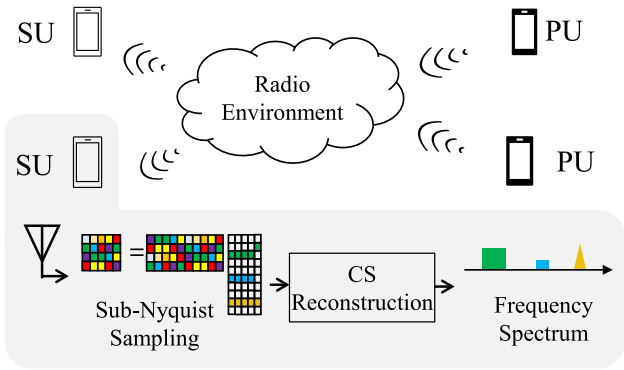


Fig. 1. Simplified illustration of compressed spectrum sensing conducted by secondary users (SUs) in a mobile cognitive radio network. The SUs conduct sub-Nyquist sampling to the received analog signal and reconstruct the primary users' (PUs) and other SUs' transmissions in the frequency domain using compressed sensing algorithms.

To address this, compressed spectrum sensing (CSS) optimizes power consumption and hardware cost by reconstructing the spectrum from sub-Nyquist time-domain samples as illurstrated in Fig. 1. The CSS comprises two steps: 1) sub-Nyquist sampling to digitize the signal at an average rate lower than the Nyquist rate, then 2) applying compressed sensing (CS) algorithms to reconstruct the frequency-domain signal [2]. Among sub-Nyquist sampling schemes, periodic nonuniform sampling (PNS) is widely studied and considered one of the most practical sampling schemes due to its scalability and simplicity [3], [4].

The *multicoset sampler* is renowned as a prominent implementation of PNS [3]. This implementation is characterized by its multiple signal lanes, each with a unique time delay. In each lane, the analog signal is digitized by an ADC at a rate far lower than the Nyquist rate. The three major hardware parameters for a multicoset sampler are a) the number of signal lanes, b) the temporal resolution of the delay control unit, and c) the relative

Manuscript received 25 April 2023; revised 30 December 2023; accepted 4 January 2024. Date of publication 12 January 2024; date of current version 6 August 2024. This work was supported by the Engineering and Physical Sciences Research Council of the United Kingdom under Grant EP/R00711X/2. Recommended for acceptance by M. Rossi. *(Corresponding author: Yue Gao.)*

Zihang Song is with the Department of Engineering, King's College London, WC2R 2LS London, U.K. (e-mail: zihang.song@kcl.ac.uk).

Yiyuan She is with the Department of Statistics, Florida State University, Tallahassee, FL 32306 USA (e-mail: yshe@stat.fsu.edu).

Jian Yang is with the China Academy of Information and Communications Technology, Beijing 100191, China (e-mail: yangjian1@caict.ac.cn).

Jinbo Peng and Yue Gao are with the School of Computer Science, Fudan University, Shanghai 200433, China (e-mail: jbpeng22@m.fudan.edu.cn; yue.gao@ieee.org).

Rahim Tafazolli is with the Institute for Communication Systems, University of Surrey, GU2 7XH, Guildford, U.K. (e-mail: r.tafazolli@surrey.ac.uk).

Digital Object Identifier 10.1109/TMC.2024.3353591

time delay coefficients in different signal lanes, collectively referred to as the *sampling pattern* [5], [6]. In a certain hardware implementation, factors a) and b) are typically predefined by the circuit layout or are inherent to the device, and the sampling pattern offer the only design flexibility, allowing adjustments to be made in software [7].

The design of the sampling pattern is crucial for successful signal reconstruction from sub-Nyquist samples acquired by a multicoset sampler because it directly decides the property of the sensing matrix in the subsequent CS reconstruction problem. An effective sampling pattern design method will improve spectrum sensing reliability and further enhance the service quality in mobile CR networks.

### A. Related Works

Sampling pattern design is usually formulated as a combinatorial optimization problem [7]. A predominant optimization target in this field is to minimize the condition number of the sensing matrix to meet the full-spark condition [5], [8], [9]. Some approaches utilize greedy-pursuit strategies to acquire locally optimal condition numbers [10]. Although one study has explored the analytical generation of full-spark sensing matrices, it specifically lacks rigorous justification [11]. However, the full-spark condition, while guaranteeing solution uniqueness, does not necessarily imply that these solutions are identifiable using current sparse approximation techniques. Additionally, its derivation assumes noise-free conditions, an ideal seldom met in practical scenarios. To mitigate the limitations of the full-spark condition, the mean-square error criterion has been proposed. However, it often incurs significant computational costs and is typically predicated on noiseless assumptions [12].

To achieve reliable signal recovery in noisy contexts, both the restricted isometry property (RIP) and the mutual incoherence property (MIP) have been introduced [13], [14], [15]. While RIP offers energy stability for sparse signal sensing matrices, its computational demands often make it less practical, leading to increased focus on MIP. The MIP is typically assessed using *mutual coherence*, a metric quantifying the maximum correlation between any two columns of a matrix. A lower bound for mutual coherence in fat matrices, known as the Welch bound, has been theoretically established [16]. Achieving this bound is crucial in compressed sensing for improved signal reconstruction and noise robustness [17], [18]. However, meeting the Welch bound can be challenging in applications requiring strict structural constraints [19]. In multicoset sampling, where sensing matrices often resemble selectively-row-chosen inverse Fourier matrices, research has focused on analytically formulating partial Fourier codebooks, utilizing tools like difference sets, to approach the Welch bound [20]. However, those partial Fourier matrices only meet the Welch bound when specific conditions on hardware parameters of the multicoset sampler are met [21].

To develop a sampling pattern design method suitable for a broader range of hardware parameters in multicoset sampling, especially for scenarios where the Welch bound is unachievable, our previous work [22] implemented a random search approach to optimize MIP. However, the study did not thoroughly delve into the complex details of the algorithm or its practical implications.

### B. Main Contributions

In this article, we consider the design of sampling patterns for multicoset sampling under a noisy condition. We approach the problem from the perspective of optimizing the MIP. Our main focus is on a broader range of hardware parameters, especially in scenarios where achieving the Welch bound might be challenging. The contributions of this article can be summarized as follows:

1) Based on the finite-field theory and some key results established by [23] [24], we derive a theorem that assures the construction of a $q \times L$ partial inverse Fourier matrix to possess an upper bound on mutual coherence at $(n-1)/\sqrt{p}$, where $q = p^a$ and $L = q^n - 1$ or $\frac{p^n-1}{p^b-1}$ with $p$ being a prime and $n$, $a$, $b$ being positive integers satisfying that $b$ divides $a$. This leads to our proposal of the finite-field-based deterministic generation (FFDG) algorithm. FFDG generates a sampling pattern in a deterministic manner to provide faithful spectrum reconstruction performance. To the authors' knowledge, FFDG is the first sampling pattern design algorithm for noise-contaminated multicoset sampling with guaranteed mutual-coherence bound.
2) By rephrasing the sampling pattern design as a mutual-coherence minimization problem, we further propose two efficient optimization algorithms: the mutual-coherence random search (MC-RS) and the mutual-coherence sequential forward selection (MC-SFS) algorithms. Both algorithms are applicable to sensing matrices of any $R \times L$ dimension. The MC-RS algorithm is particularly efficient when $R$ is significantly smaller than $L/2$. It successfully identifies a nearly optimal solution with high probability within a search space of size $\binom{L}{R}$, with a time complexity of $O(L^2Rm)$, where $m$ is significantly smaller than $\binom{L}{R}$. The MC-SFS algorithm provides improved efficiency for larger $R$ values comparable to $L/2$. It employs a greedy pursuit strategy to discover a locally optimal solution within a time complexity of $O(L^3R^2)$.
3) We further develop MC-RS into the restricted-mutual-coherence random search (RMC-RS) algorithm, aimed at minimizing a constrained form of the mutual coherence of the sensing matrix. RMC-RS particularly works between consecutive spectrum sensing windows to yield a dynamically adjusted sampling pattern. RMC-RS shows extremely low time complexity and strong adaptability to the spectrum support.

### C. Outline

The rest of this article is organized as follows. The mathematical models of the signal and the multicoset sampler, as well as the definitions of RIP and MIP restrictions on sensing matrices, are introduced in Section II. Moreover, we show why MIP is a desirable property of the sensing matrix to recover wideband signal with noise when using simultaneous orthogonal matching pursuit (SOMP). In Section III, the FFDG algorithm is

TABLE I
NOTATION

| | |
|---|---|
| $x(t)$ | continuous-time baseband complex signal |
| $f_{\text{Nyq}}$ | the Nyquist frequency of $x(t)$ |
| $T$ | $1/f_{\text{Nyq}}$ |
| $k$ | number of non-zero subbands of $x(t)$ |
| $L$ | number of subbands in $[0, f_{\text{Nyq}}]$ |
| $R$ | number of cosets in a multicoset sampler |
| $c_r$ | delay coefficient in the $r$th coset |
| $\mathcal{C}$ | sampling pattern |
| $x_{c_r}[n]$ | discrete sampling points in the $r$th coset |
| $\mathcal{S}$ | the row indexes of $\mathbf{X}$ that are non-identically zero |
| $\hat{\mathcal{S}}$ | estimation of $\mathcal{S}$ |
| $\mathbf{Y}$ | measurement of a multicoset sampler |
| $\mathbf{X}^*$ | spectrum matrix to be estimated |
| $\mathbf{W}$ | additive noise to the measurement |
| $\mathbf{A}$ | multicoset sensing matrix |
| $\mathbf{X}$ | the approximation of $\mathbf{X}^*$ |
| $\|\cdot\|_0$, $\|\cdot\|_2$, $\|\cdot\|_{\text{F}}$ | $\ell_0$, $\ell_2$ and Frobenius norm |
| $\|\cdot\|_{2,0}$ | $\ell_{2,0}$ norm (the number of non-zero rows) |
| $\cdot^{\text{H}}$ | the conjugate transpose of a matrix |
| $\cdot^{\dagger}$ | the pseudo inverse of a matrix |
| $A_{i,j}$ | the $\{i,j\}$th element of matrix $\mathbf{A}$ |
| $\mathbf{A}_i$ | the $i$th column vector of matrix $\mathbf{A}$ |
| $\mathbf{A}_{\mathcal{S}}$ | submatrix of $\mathbf{A}$ composed of columns indexed by $\mathcal{S}$ |

presented to generate a sampling pattern with strict MIP control. Two optimization algorithms, namely MC-RS and MC-SFS, are then presented to minimize the mutual coherence of the sensing matrix. In Section IV, the RMC-RS algorithm is described to design the sampling pattern between consecutive spectrum sensing windows iteratively. Numerical experiments are demonstrated in Section V. Common notation, as summarized in Table I, is used throughout the article.

## II. Mathematical Models

### A. Signal Model

We consider a complex analog signal $x(t)$ defined within the frequency range $[0, B]$. The signal consists of $N_{\text{Sig}}$ distinct transmissions, mathematically expressed as:

$$x(t) = \sum_{i=1}^{N_{\text{Sig}}} s_i(t). \tag{1}$$

Each of these transmissions, denoted by $s_i(t)$ for $i = 1, 2, \ldots, N_{\text{Sig}}$, has a bandwidth that does not exceed $B/L$, where $L$ is a positive integer.

The model is based on the assumption that $N_{\text{Sig}} \ll L$. This implies that the frequency spectrum of $x(t)$ is sparse in the range $[0, B]$. To further formulate this sparsity, we divide the frequency range $[0, B]$ into $L$ equal subbands. Let $k$ denote the number of these subbands that are actually occupied by active transmissions. Under our assumptions, $k$ is bounded as follows:

$$k \leq 2N_{\text{Sig}}. \tag{2}$$

We refer to $k$ as the spectrum sparsity level of $x(t)$ within the frequency range $[0, B]$. It follows from our assumptions that $k \ll L$.

To set the context for the Nyquist frequency $f_{\text{Nyq}}$, we first note that the signal $x(t)$ is a complex baseband signal defined within the frequency range $[0, B]$. In this case, the Nyquist frequency is directly given by the upper bound of this frequency range. Specifically, we have $f_{\text{Nyq}} = B$. We define $T$ as the Nyquist interval, formally expressed as $T \triangleq 1/f_{\text{Nyq}}$.

### B. Multicoset Sampling

The basic structure of a multicoset sampler is illustrated in Fig. 2(a). The analog input $x(t)$ is first divided into $R$ signal lanes by an $R$-way power splitter ($R < L$). For each signal lane $r$ ($r = 1, \ldots, R$), also referred to as a 'coset', a unique time delay of $c_r T$ is applied directly to the analog signal, where $c_r$ is an integer coefficient. The set of all $R$ delay coefficients is referred to as the 'sampling pattern' and is denoted by $\mathcal{C}$ as

$$\mathcal{C} \triangleq \{c_1, \ldots, c_R\} \subseteq \{1, 2, \ldots, L\},$$

with $|\mathcal{C}| = R$.

Subsequently, the analog signal in each coset is sampled by an ADC running at rate $f_{\text{s}} \triangleq f_{\text{Nyq}}/L$. The sampling clocks for all the cosets are synchronized and strictly aligned.

Letting the sampling window length be $N/f_{\text{s}}$, the discrete sample sequence acquired in the $r$th coset is

$$x_r[n] = x\left(\frac{nL}{f_{\text{Nyq}}} + \frac{c_r}{f_{\text{Nyq}}}\right), \quad n = 1, 2, \ldots, N. \tag{3}$$

A multicoset sampler obeys the following measuring process [22]:

$$\mathbf{Y} = \mathbf{A}\mathbf{X}^* + \mathbf{W}, \tag{4}$$

where $\mathbf{Y} \in \mathbb{C}^{R \times N}$ is the measurement with

$$Y_{r,n} = LTe^{-j2\pi c_r n/(LN)} \sum_{i=1}^{N} x_r[i] e^{-j2\pi ni/N}, \tag{5}$$

and $\mathbf{A} \in \mathbb{C}^{R \times L}$ is the sensing matrix with

$$A_{r,l} = e^{j2\pi c_r \frac{(l-1)}{L}}, \tag{6}$$

and $\mathbf{X}^* \in \mathbb{C}^{L \times N}$ corresponds to the $LN$-points discrete Fourier transform of the discrete version of $x(t)$ by

$$X^*_{l,n} = \sum_{\tau=1}^{LN} x\left(\frac{\tau}{f_{\text{Nyq}}}\right) e^{-j2\pi \frac{(l-1)N+n}{LN}}, \tag{7}$$

and $\mathbf{W}$ is the additive noise caused by multiple factors such as channel noise and internal thermal noise of the receiver devices.

### C. Desired Isometry and Incoherence on Sensing Matrices

Owing to the block-sparse property of the wideband signal spectrum, $\mathbf{X}^*$ can be treated as a row-sparse matrix composed of jointly sparse vectors. When the measurement $\mathbf{Y}$ contains noise, finding the optimal sparse approximation to $\mathbf{X}^*$ in (4)

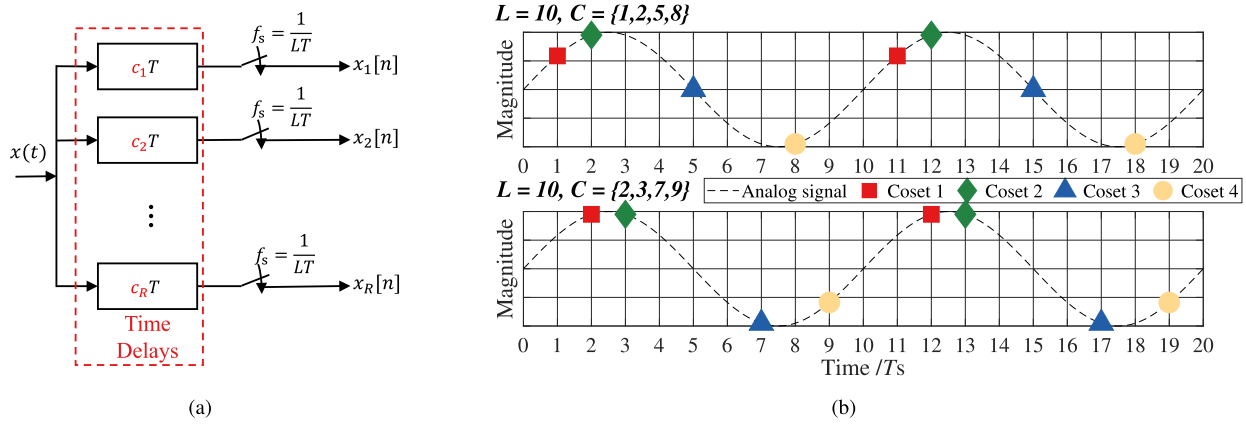


Fig. 2. (a) Diagram of the basic implementation of a multicoset sampler. (b) Examples of periodic nonuniform samples on an input sine wave produced by a multicoset sampler with $L = 10$ and $R = 4$. The sampling pattern is $\mathcal{C} = \{1, 2, 5, 8\}$ for the top graph and $\mathcal{C} = \{2, 3, 7, 9\}$ for the bottom one.

can be characterized as a *simultaneous sparse approximation problem* [25]

$$\arg\min_{\mathbf{X}\in\mathbb{C}^{L\times N}} \|\mathbf{X}\|_{2,0} \text{ subject to } \|\mathbf{Y}-\mathbf{A}\mathbf{X}\|_{\mathsf{F}} < \epsilon, \tag{8}$$

where $\|\cdot\|_{2,0}$ is the standard notation to denote the number of non-zero rows, and $\epsilon$ is a small constraint of the noise.

Directly solving problem (8) is notably intractable because $\|\cdot\|_{2,0}$ is non-convex and lack of continuous gradient. Fortunately, some approaches are proposed to acquire a sub-optimal solution to the problem. The first type of approximation is characterized by $\ell_1$-relaxation such as multiple basis pursuit denoising [26], [27] and group-Lasso [28], [29], [30], [31]. For systems that require high real-time performance, greedy pursuit algorithms, typically the SOMP algorithm, are widely used owing to their computational efficiency and scalability [25].

Various constraints can be imposed on the sensing matrix to ensure the statistical estimation accuracy of the solution. A widely-known restriction is the RIP [13], defined as:

*Definition 1 (Restricted Isometry Property):* The sensing matrix $\mathbf{A}$ satisfies the restricted isometry property of order $k$ with parameter $\delta_k$ when there exists $\delta_k \in [0, 1)$, such that

$$(1-\delta_k)\|\mathbf{x}\|_2^2 \le \|\mathbf{A}\mathbf{x}\|_2^2 \le (1+\delta_k)\|\mathbf{x}\|_2^2 \tag{9}$$

for all $\{\mathbf{x} : \|\mathbf{x}\|_0 \le k\}$.

Particularly, RIP can ensure faithful support recovery through SOMP-like algorithms [32], [33], [34]. However, verifying RIP for a specific sensing matrix is computationally difficult in practice. In this sense, MIP offers a computationally more accessible proxy for RIP [14].

*Definition 2 (Mutual Incoherence Property):* The mutual coherence of the matrix $\mathbf{A} \in \mathbb{C}^{R\times L}$ is defined as

$$\mu(\mathbf{A}) \triangleq \max_{i\neq j} \frac{|\langle \mathbf{A}_i, \mathbf{A}_j\rangle|}{\|\mathbf{A}_i\|_2 \|\mathbf{A}_j\|_2}, \tag{10}$$

where $\mathbf{A}_i$ and $\mathbf{A}_j$ denote the $i$th and $j$th columns (atoms) of matrix $\mathbf{A}$.

It can be elucidated that RIP and MIP are intrinsically related, as evidenced by their relationship shown in the equation (e.g., see (IV.7) in [35]):

$$\delta_k \le (k-1)\mu(\mathbf{A}). \tag{11}$$

The mutual coherence $\mu(\mathbf{A})$ quantifies the maximal correlation strength between any two columns (atoms) of the sensing matrix $\mathbf{A}$. Intuitively, RIP is satisfied with high probability when $\mu(\mathbf{A})$ is relatively small. The MIP condition ensuring exact recovery through $\ell_1$-optimization techniques has been derived in [14], expressed as:

$$k < \frac{1}{2}\left(\frac{1}{\mu(\mathbf{A})}+1\right). \tag{12}$$

Other algorithms, such as Lasso, basis pursuit, and hard thresholding pursuit, have also been influenced by the properties of the sensing matrix, demonstrating variances in recovery efficacy based on mutual coherence and other matrix characteristics [29], [36], [37], [38], [39], [40], [41]. However, considering the demands of spectrum sensing, where rapid real-time responses are required, our study predominantly employs the SOMP-type algorithm. This leads to a detailed examination of the relationship between the MIP of the sensing matrix and the statistical accuracy of support recovery.

Given an initial residual $\mathbf{R}^{(0)} = \mathbf{Y}^{R\times N}$ and an empty initial support $\hat{\mathcal{S}}^{(0)}$, starting at $t = 1$, SOMP iterates

$$\hat{s}^{(t)} = \arg\max_s \{\|\mathbf{A}_s^{\mathsf{H}} \cdot \mathbf{R}^{(t-1)}\|_{\mathsf{F}}, s \notin \hat{\mathcal{S}}^{(t-1)}\}, \tag{13a}$$

$$\hat{\mathcal{S}}^{(t)} = \hat{\mathcal{S}}^{(t-1)} \cup \hat{s}^{(t)}, \tag{13b}$$

$$\mathbf{X}^{(t)} = \mathbf{O}^{L\times N}, \mathbf{X}[t, \hat{\mathcal{S}}^{(t)}] = \mathbf{A}^{\dagger}_{\hat{\mathcal{S}}^{(t)}}\mathbf{Y}, \tag{13c}$$

$$\mathbf{R}^{(t)} = \mathbf{Y} - \mathbf{A}\mathbf{X}^{(t)}, \tag{13d}$$

where $\mathbf{X}[t, \hat{\mathcal{S}}^{(t)}]$ denotes the rows of $\mathbf{X}^{(t)}$ indexed by $\hat{\mathcal{S}}^{(t)}$ and $\mathbf{R}^{(t)}$ denotes the residual in the $t$th iteration. The algorithm is halted either by fixing the number of iterations or by imposing a threshold on the residual.

Step (13a) in SOMP is referred to as the *greedy selection* [42]. In a noise-free setup, it is proved that when $\mu(\mathbf{A}) < 1/(2\tilde{k})$, if

the residual given by SOMP in the $t$th iteration satisfies

$$\|\mathbf{R}^{(t)}\|_{\mathsf{F}} \leq \left[1 + Nk\frac{1-k\mu(\mathbf{A})}{(1-2k\mu(\mathbf{A}))^2}\right]^{1/2}\epsilon_0, \tag{14}$$

where $\epsilon_0$ is a small error bound, it follows that the atoms chosen so far are optimal, namely $\hat{\mathcal{S}}^{(t)} \subset \mathcal{S}$.

In a noisy setup, we show intuitively how mutual coherence could diminish the accuracy of greedy selections. The residual calculated by step (13d) in the $t$th iteration is detailed as

$$\begin{aligned}\mathbf{R}^{(t)} &= \mathbf{R}^{(0)} - \mathbf{P}\left[\mathbf{A}_{\hat{\mathcal{S}}^{(t)}}\right]\mathbf{R}^{(0)} \\ &= \mathbf{R}^{(t-1)} - \mathbf{P}\left[\mathbf{A}_{\hat{\mathcal{S}}^{(t)}}\right]\mathbf{R}^{(t-1)},\end{aligned} \tag{15}$$

where

$$\mathbf{P}\left[\mathbf{A}_{\hat{\mathcal{S}}^{(t)}}\right] \triangleq \mathbf{A}_{\hat{\mathcal{S}}^{(t)}}(\mathbf{A}^{\mathsf{H}}_{\hat{\mathcal{S}}^{(t)}}\mathbf{A}_{\hat{\mathcal{S}}^{(t)}})^{-1}\mathbf{A}^{\mathsf{H}}_{\hat{\mathcal{S}}^{(t)}} \tag{16}$$

defines the projection matrix of size $R \times R$. This matrix projects any vector (or the columns of a matrix) in $\mathbb{C}^R$ onto the column space of $\mathbf{A}_{\hat{\mathcal{S}}^{(t)}}$, which represents the subspace spanned by the currently selected set of atoms up to the $t$th iteration. We apply the Schmidt orthogonalization to the atoms in $\mathbf{A}_{\hat{\mathcal{S}}^{(t)}}$ in reverse order as

$$\begin{aligned}\mathbf{B}_t &= \mathbf{A}_{\hat{s}^{(t)}}, \\ \mathbf{B}_{t-1} &= \mathbf{A}_{\hat{s}^{(t-1)}} - \mathbf{P}\left[\mathbf{A}_{\hat{s}^{(t)}}\right]\mathbf{A}_{\hat{s}^{(t-1)}}, \\ &\cdots \\ \mathbf{B}_1 &= \mathbf{A}_{\hat{s}^{(1)}} - \sum_{i=2}^{t}\mathbf{P}\left[\mathbf{A}_{\hat{s}^{(i)}}\right]\mathbf{A}_{\hat{s}^{(1)}}.\end{aligned} \tag{17}$$

where

$$\mathbf{P}\left[\mathbf{A}_{\hat{s}^{(t)}}\right] \triangleq \mathbf{A}_{\hat{s}^{(t)}}(\mathbf{A}^{\mathsf{H}}_{\hat{s}^{(t)}}\mathbf{A}_{\hat{s}^{(t)}})^{-1}\mathbf{A}^{\mathsf{H}}_{\hat{s}^{(t)}} \tag{18}$$

is a projection matrix of size $R \times R$ which projects any vector in $\mathbb{C}^R$ onto the span of vector $\mathbf{A}_{\hat{s}^{(t)}}$, the selected atom in the $t$th iteration. Then (15) can be rewritten as

$$\mathbf{R}^{(1)} = \mathbf{R}^{(0)} - \mathbf{P}\left[\mathbf{A}_{\hat{s}^{(1)}}\right]\mathbf{R}^{(0)}, \tag{19a}$$

$$\mathbf{R}^{(t)} = \mathbf{R}^{(t-1)} - \underbrace{\mathbf{P}\left[\mathbf{A}_{\hat{s}^{(t)}}\right]\mathbf{R}^{(t-1)}}_{a(t)} - \underbrace{\sum_{i=1}^{t-1}\mathbf{P}\left[\mathbf{B}_i\right]\mathbf{R}^{(t-1)}}_{e(t)}, (t \geq 2). \tag{19b}$$

In (19b), two projection terms, $a(t)$ and $e(t)$, are subtracted from $\mathbf{R}^{(t-1)}$ to update the residual. Specifically, $a(t)$ represents the projection of $\mathbf{R}^{(t-1)}$ on $\mathbf{A}_{\hat{s}^{(t)}}$, and $e(t)$ is the cumulative projection of $\mathbf{R}^{(t-1)}$ on each of the previous Schmidt vectors $\mathbf{B}_1, \ldots, \mathbf{B}_{t-1}$.

The term $e(t)$ acts as a residual error, affecting the accuracy in estimating $\mathbf{R}^{(t)}$. From a preliminary analysis, we derive a loose upper bound for the Frobenius norm of this error as:

$$\|e(t)\|_{\mathsf{F}} \leq \sum_{i=1}^{t-1}\left\|\mathbf{P}\left[\mathbf{B}_i\right]\mathbf{R}^{(t-1)}\right\|_{\mathsf{F}} \leq \mu(\mathbf{A})\sum_{i=1}^{t-1}\left\|\mathbf{R}^{(t-1)}\right\|_{\mathsf{F}}. \tag{20}$$

A smaller value of $\mu(\mathbf{A})$ imposes a tighter constraint on the absolute magnitude of the error term. For instance, in an extreme case where $\mu(\mathbf{A}) \to 0$ (meaning $\mathbf{A}$ is nearly orthogonal), we have $e(t) \to 0$, leading to a more accurate $\mathbf{R}^{(t)}$ and thus a more reliable identification of $\hat{s}^{(t)} \in \mathcal{S}$. Additionally, it is evident that the accumulated effect of the error term, $e(t)$, increases with growing $t$. Fig. 3 illustrates the probability of $\hat{s}^{(t)}$ being part of $\mathcal{S}$ over the first five iterations of SOMP, comparing three sets of sensing matrices characterized by different $\mu(\mathbf{A})$ ranges. This figure shows the relationship between the accumulation of $e(t)$ across iterations and the proficiency of SOMP in correctly identifying an element from the support set. As $\mu(\mathbf{A})$ decreases, this probability drops at a faster rate.

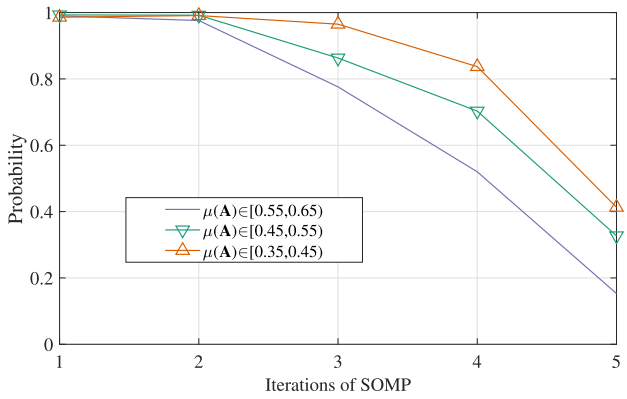


Fig. 3. Probabilities of correctly finding the entry of a non-zero row of $\mathbf{X}$ in each of the first five iterations of SOMP.

## III. Sampling Pattern Design Toward Minimal MIP

The multicoset sensing matrix $\mathbf{A}$ is constructed as a partial inverse Fourier matrix by retaining the rows indexed by $\mathcal{C}$, which can be formally represented as

$$\mathbf{A} = (\mathcal{F}^L)^{-1}_{\mathcal{C}}, \tag{21}$$

where $(\mathcal{F}^L)^{-1}$ is an $L \times L$ inverse Fourier matrix with its $\{i,k\}$th element given by $\exp(2\pi jik/L)$. Here, $\mathcal{C}$, with $|\mathcal{C}| = R$, is the set of row indices corresponding to the sampling pattern of the multicoset sampler. For specific hardware implementations, the values of $L$ and $R$ are often fixed by the resolution of the time-delay unit and the number of physical signal lanes. Thus, in our setup, the indices in $\mathcal{C}$ are the most critical parameters that influence the design of multicoset sensing matrices.

The sensing matrix $\mathbf{A}$, generated by a sampling pattern $\mathcal{C}$ chosen from $\{0, 1, \ldots, L-1\}$ in a uniformly random manner, is shown to satisfy RIP$(k, \delta_k)$ with high probability [36] when

$$k \leq c(\delta_k) \cdot \frac{R}{\log^4 L}, \tag{22}$$

where $c(\delta_k)$ is a coefficient that depends only on $\delta_k$. However, sampling patterns generated uniformly are not always reliable since (22) does not provide a deterministic condition.

### A. Creating Sampling Patterns With Controlled MIP Threshold

We first present a deterministic construction method for generating sampling patterns, leading to a sensing matrix with an explicitly bounded mutual coherence. Our approach is based on the principles of finite field theory. To provide context, Devore et al. utilized finite field theory in their influential 2007 study [15] to design binary sensing matrices with dimensions of $p^2 \times p^{n+1}$. These matrices exhibit the RIP up to an order $2k$, under the condition

$$k < \frac{p}{2(n-1)} + \frac{1}{2}, \tag{23}$$

where $p$ is a prime number and $n < p$ stands for a positive integer. Xu et al. proposed a deterministic design method for partial Fourier matrices using the finite field theory [24]. Hereon, we extended the finite field theory to the design of a partial inverse Fourier matrix satisfying MIP.

Denote $q = p^a$ as a prime power, with $p$ being a prime and $a$ a positive integer. The finite field $\mathbb{F}_q$ comprises $q$ elements. Extending this, we characterize $\mathbb{F}_{q^n}$ as the finite field with $q^n$ elements, described by:

$$\mathbb{F}_{q^n} = \left\{ \sum_{i=0}^{n-1} a_i \alpha \ : \ a_i \in \mathbb{F}_q \right\}, \tag{24}$$

with $\alpha$ as a zero of an irreducible polynomial within $\mathbb{F}_q[x]$. We then introduce $g$ as a primitive root of $\mathbb{F}_{q^n}$, leading to our foundational theorem:

*Theorem 1:* For a prime power $q = p^a$, with $p$ being prime and $a$ a positive integer, let either $L = q^n - 1$ or $L = \frac{p^n-1}{p^b-1}$ be true, where $n$ is a positive integer and $b|a$. If

$$\mathcal{C} = \{\log_g(t-\alpha) \mod L \mid t \in \mathbb{F}_q\}, \tag{25}$$

then the partial inverse Fourier matrix $\mathbf{A} = (\mathcal{F}^L)^{-1}_{\mathcal{C}}$ has a mutual coherence bound:

$$\mu(\mathbf{A}) \le \frac{n-1}{\sqrt{p}}. \tag{26}$$

*Proof:* The proof of Theorem 1 is inspired by [24] and relies on a theorem in number theory [23]. This theorem is presented as a lemma without its proof.

*Lemma 1:* Let $\chi$ be any nontrivial complex-valued multiplicative character of $\mathbb{F}^*_{q^n}$, and $\alpha$ an element in $\mathbb{F}_{q^n}$ that generates $\mathbb{F}_{q^n}$ over $\mathbb{F}_q$. Then

$$\left| \sum_{t \in \mathbb{F}_q} \chi(t-\alpha) \right| \le (n-1)\sqrt{q}. \tag{27}$$

Denote

$$\mathcal{C} = \{c_i = \log_g(t_i - \alpha) : i = 1, \ldots, q\}$$

as a sampling pattern designed following Theorem 1, where $t_i$ is the $i$th element in $\mathbb{F}_q$. For any two column indexes $l_1, l_2 \in \{1, \ldots, L\}$ and $l_1 \neq l_2$, the inner product of the $l_1$th and $l_2$th atoms of the matrix $\mathbf{A}$ is

$$\begin{aligned} \langle \mathbf{A}_{l_1}, \mathbf{A}_{l_2} \rangle &= \sum_{i=0}^{p-1} e^{j2\pi c_i \frac{l_1-1}{L}} e^{-2\pi j c_i \frac{l_2-1}{L}} \\ &= \sum_{i=0}^{p-1} e^{j2\pi c_i \frac{l_1-l_2}{L}} \\ &= \sum_{i=0}^{p-1} e^{j2\pi \log_g(t_i-\alpha)\frac{l_1-l_2}{L}}. \end{aligned} \tag{28}$$

Define $\chi(t_i - \alpha) = e^{j2\pi \log_g(t_i-\alpha)\frac{l_1-l_2}{L}}$. It can be easily verified that $\chi(t_i - \alpha)$ is a nontrivial multiplicative character of $\mathbb{F}^*_{q^n}$ because $\log_g(t_i - \alpha) < q^n - 1$, $L = q^n - 1$ and $1 \le |l_1 - l_2| \le L - 1$. By Lemma 1, we have

$$\langle \mathbf{A}_{l_1}, \mathbf{A}_{l_2} \rangle = \sum_{t \in \mathbb{F}_q} \chi(t-\alpha). \tag{29}$$

Thus,

$$\begin{aligned} \mu(\mathbf{A}) &= \max_{1 \le i < j \le L} \frac{|\langle \mathbf{A}_i, \mathbf{A}_j \rangle|}{\|\mathbf{A}_i\|_2 \|\mathbf{A}_j\|_2} \\ &= \frac{1}{q} \max_{1 \le i < j \le L} |\langle \mathbf{A}_i, \mathbf{A}_j \rangle| \\ &\le \frac{n-1}{\sqrt{q}}. \end{aligned} \tag{30}$$

The proof is complete.

Based on Theorem 1, we introduce the FFDG algorithm, which is detailed in Algorithm 1.

**Algorithm 1:** Finite-Field-Based Deterministic Generation (FFDG).

**Input:** $L$ satisfying (31) or (32); $R$ satisfying (33)
**Output:** $\mathcal{C}$
1: Construct a finite field $\mathbb{F}_R$ using (24)
2: Identify an irreducible polynomial $p(x)$ in $\mathbb{F}_R[x]$ and a zero $\alpha$
3: Create a finite field $\mathbb{F}_{R^n}$ as $\mathbb{F}_{R^n} = \mathbb{F}_R[x]/p(x)$
4: Determine a primitive root $g$ in $\mathbb{F}_{R^n}$
5: Calculate $\mathcal{C} \leftarrow \{\log_g(t-\alpha) \mod L \mid t \in \mathbb{F}_R\}$

In Step 2, an irreducible polynomial can be identified by enumerating a few elements from $\mathbb{F}_q$.In Step 4, a practical approach to identifying a primitive root in a finite field is described by [43]. This method is based on the principle that $g$ is a primitive root in $\mathbb{F}_{q^n}$ if $g^{\frac{q^n-1}{\mathcal{L}}} \neq 1$ for each prime divisor $\mathcal{L}$ of $q^n - 1$. As for step 5, the logarithm of $u$ in $\mathbb{F}^*_{q^n}$ is derived as $\log_g u = i\sqrt{q^n - 1} + j$ for pairs $\{i, q\}$ that satisfy $ug^{-j(q^n-1)} = g^i$ [44].

When deploying FFDG, certain conditions are imposed on multicoset parameters. Specifically, $L$ needs to satisfy:

$$L = q^n - 1 \tag{31}$$

or

$$L = \frac{q^n - 1}{p^b - 1} \tag{32}$$

with $q = p^a$ being a prime power and $n, a, b$ being positive integers satisfying $b|a$. The coset number $R$ must obey:

$$R = q. \tag{33}$$

As deduced from (12) and (26), the sensing matrix $\mathbf{A}$ generated by FFDG is able to recover a $k$-sparse signal under the condition:

$$k < \frac{\sqrt{R}}{2(n-1)} + \frac{1}{2}. \tag{34}$$

It is noteworthy that this threshold aligns with the one presented in the deterministic design of binary sensing matrices by DeVore [15]. Our methodology is not limited to the sensing matrices design of multicoset samplers but extends to broader CSS applications.

### B. Sampling Pattern Construction by Optimization

In this subsection, we focus on the design of sampling patterns without constraining $L$ and $R$. For a given pair $(L, R)$, there are $\binom{L}{R}$ potential sampling patterns. Rather than seeking a universally optimal solution, our aim is to identify a sampling pattern $\mathcal{C}$ that facilitates the task of recovery algorithms in distinguishing signal components located in different frequency bands. We follow the principle of minimizing the mutual coherence but introduce a new 'min-max' optimization criterion. Specifically, we aim at the objective problem:

$$\arg\min_{\mathcal{C}\subset\{0,1,\ldots,L-1\}} \max_{\Delta l\in\{1,\ldots,L-1\}} f_L(\mathcal{C}) \quad \text{s.t. } |\mathcal{C}| = R, \tag{35}$$

where

$$f_L(\mathcal{C}) = \sum_{\substack{c_1,c_2\in\mathcal{C},\\ c_1<c_2}} \cos\left(\frac{2\pi(c_1-c_2)\Delta l}{L}\right). \tag{36}$$

It is obvious that solving (35) also minimizes $\mu(\mathbf{A})$ given

$$\mu(\mathbf{A}) = \max_{\Delta l\in\{1,\ldots,L-1\}} \frac{1}{R}\sqrt{R + 2f_L(\mathcal{C})}. \tag{37}$$

Problem (35) is a nonconvex discrete nonlinear optimization problem, which is NP-hard. In this perspective, the random search strategy [45] shows the ability to operate without the need for gradient information. Random search operates by progressively moving to preferable positions within the search space. With the assumption that the spectrum support remains unknown, the search space for problem (35) is defined as all $\mathcal{C} \in \{1, 2, \ldots, L\}$ with $|\mathcal{C}| = R$. The primary objective is to find a $\mathcal{C}$ that results in a value for $\mu(\mathbf{A})$ that is nearly minimal.

Building on our prior work [22], where a foundational random search strategy for MIP minimization was introduced, we further refine and extend this approach. We hereby propose the MC-RS algorithm for sampling pattern design, detailed in Algorithm 2. This new approach dives deeper into the algorithmic intricacies and offers more comprehensive solutions for practical scenarios.

**Algorithm 2:** Mutual-Coherence Random Search (MC-RS).

**Input:** $L$; $R$; $m$
**Output:** $\mathcal{C}$
1: $t \leftarrow 1$, $f_{L\min} \leftarrow \infty$
2: **while** $t \le m$ **do**
3: select $\mathcal{C}^{(t)} \subset \{0, 1, \ldots, L-1\}$ with $|\mathcal{C}^{(t)}| = R$ in a uniformly random manner
4: $f_L^{(t)} = \max_{\Delta l\in\{1,\ldots,L-1\}} \sum_{\substack{c_1,c_2\in\mathcal{C}^{(t)},\\ c_1<c_2}} \cos(\frac{2\pi(c_1-c_2)\Delta l}{L})$
5: **if** $f_L^{(t)} < f_{L\min}$ **then**
6: $\mathcal{C} \leftarrow \mathcal{C}^{(t)}$
7: **end if**
8: $t = t + 1$
9: **end while**

The input parameter $m$ indicates the number of iterations that the MC-RS algorithm conducts to generate a decent solution. Fortunately, a large value of $m$ is often unnecessary for MC-RS to yield a design with a good value of $\mu(\mathbf{A})$. First, given $L = 37$ and $R = 7$, we show the cumulative distribution function (CDF) of $\mu(\mathbf{A})$ corresponding to all the $\binom{37}{7}$ sampling patterns in Fig. 4(a). About 5 percent of the values are distributed in the range [0,0.45), and about 0.2 percent of the values are distributed in the range [0,0.4). By seeking $m = 100$ we have about 99.4% chance to get a pattern yielding $\mu(\mathbf{A}) < 0.45$; by $m = 1000$ we have nearly 100% chance to get $\mu(\mathbf{A}) < 0.45$ and 86.5% chance to get $\mu(\mathbf{A}) < 0.4$. Compared to $\binom{37}{7} = 10,295,472$, a relatively small $m$ can already guarantee a nearly optimal solution with overwhelming probability. Similar distributions and conclusions hold for other combinations of $L$ and $R$. By taking $L = 34, 35, 36, 37$ and $R = 4, 5, 6, 7, 8$, the frequencies of $\mu(\mathbf{A})$ within the smallest 1% values between the minimum and the maximum are shown in Fig. 4(b). Our experiments reveal a nearly logarithmic linear relationship between $L$ and $R$, indicating that $m \sim 2^R$ is sufficient to ensure a stable probability of finding a sampling pattern with a favorable $\mu(\mathbf{A})$.

The MC-RS algorithm employs a random grid search strategy, efficiently searching the solution space to identify a robust suboptimal solution with high probability within a manageable number of iterations. The algorithm is designed to handle complex scenarios, offering flexibility and adaptability in its operation. However, like all random-search-based algorithms, it holds an inherent feature of randomness which, while effectively covering a broad search space, leads to an expansive search complexity as $L$ and $R$ increase (assuming a constant compressed sampling ratio $R/L$).

We further present the MC-SFS algorithm, another novel approach based on a greedy pursuit strategy. The MC-SFS algorithm is structured to acquire a local optimum within a polynomial time complexity, as detailed in Algorithm 3.

To construct the sensing matrix $\mathbf{A}$, MC-SFS operates by iteratively selecting rows from the inverse Fourier matrix $(\mathcal{F}^L)^{-1}$. In each iteration, Step 4 ensures that the matrix composed of the selected rows exhibits the minimum mutual coherence. Given $L$ and $R$, the sampling pattern designed by MC-SFS always

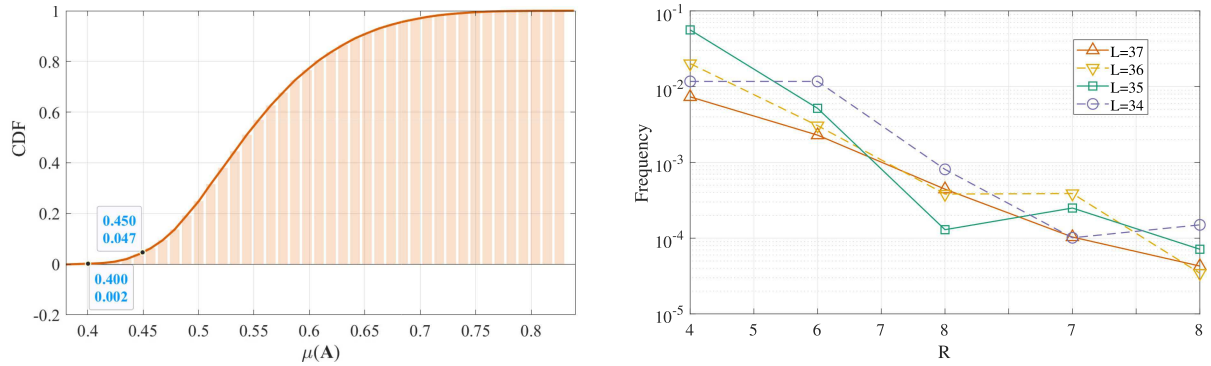


Fig. 4. (a) Distribution of $\mu(\mathbf{A})$ by examining all the sampling patterns given $L = 37$ and $R = 7$, (b) the frequencies of $\mu(\mathbf{A})$ within the smallest 1% values between the minimum and the maximum.

**Algorithm 3:** Mutual-Coherence Sequential Forward Selection (MC-SFS).

**Input:** $L$; $R$
**Output:** $\mathcal{C}$
1: $t \leftarrow 2, \mathcal{C} \leftarrow \varnothing$
2: uniformly select $c^{(1)}$ from $\{1, \ldots, L\}$, $\mathcal{C}^{(1)} \leftarrow \varnothing \cup c^{(1)}$
3: **while** $t \leq R$ **do**
4: $\quad c^{(t)} = \arg\min_{c \in \{0,1,\ldots,L-1\}} f_L(\mathcal{C}^{(t-1)} \cup c)$
5: $\quad \mathcal{C}^{(t)} \leftarrow \mathcal{C}^{(t-1)} \cup c^{(t)}$
6: $\quad t \leftarrow t + 1$
7: **end while**
8: $\mathcal{C} \leftarrow \mathcal{C}^{(R)}$

produces an explicitly controlled mutual coherence $\mu(\mathbf{A})$. Importantly, the resulting $\mu(\mathbf{A})$ is unaffected by the initial choice in Step 2, despite the output sampling pattern of MC-SFS being a local optimizer.

## IV. Dynamic Adjustment of Sampling Patterns in Consecutive Cognition Cycles

Spectrum sensing is continuously conducted by CR devices to obtain the latest spectrum occupancy. The time period from the beginning of one spectrum sensing window to the beginning of the next one is often referred to as a *cognition cycle* [46]. Between consecutive cognition cycles, the sampling pattern can be set as either fixed or dynamic. The latter provides better robustness to the dynamics of the spectrum support. In this section, we propose a dynamic sampling pattern adjustment strategy with reduced computational complexity and improved performance.

Our proposal is based on a basic assumption of CR that the cognition cycle rate is much faster than the average rate of change of the spectrum support, which is the essential prerequisite to ensure successful spectrum access. In other words, the spectrum support is unlikely to undergo significant changes between two consecutive cognition cycles. Denoting the spectrum support recovered by the last previous cognition cycle as $\hat{\mathcal{S}}_{\text{Last}}$, we can use $\hat{\mathcal{S}}_{\text{Last}}$ as the prior rough estimate of the genuine spectral support $\mathcal{S}$ of the current cognition cycle.

**Algorithm 4:** Restricted-Mutual-Coherence Random Search (RMC-RS).

**Input:** $L$; $R$; $m$; $\hat{\mathcal{S}}_{\text{Last}}$
**Output:** $\mathcal{C}$
1: $t \leftarrow 1, \mu_{\mathcal{I}\min} \leftarrow 1, \mathcal{I} \leftarrow \hat{\mathcal{S}}_{\text{Last}}$
2: **while** $t \leq m$ **do**
3: $\quad$ select a pattern $\mathcal{C}^{(t)}$ with $|\mathcal{C}^{(t)}| = R$
4: $\quad$ calculate $\mathbf{A}$ according to (6) with $\mathcal{C}^{(t)}$
5: $\quad$ calculate $\mu_{\mathcal{I}}(\mathbf{A})$ according to (38)
6: $\quad$ **if** $\mu_{\mathcal{I}}(\mathbf{A}) < \mu_{\mathcal{I}\min}$ **then**
7: $\quad\quad \mathcal{C} \leftarrow \mathcal{C}^{(t)}$
8: $\quad$ **end if**
9: $\quad t = t + 1$
10: **end while**

Define a restricted version of mutual coherence as follows:

*Definition 3 (Restricted Mutual Coherence):* The restricted mutual coherence of matrix $\mathbf{A} \in \mathbb{C}^{p \times L}$ with index set $\mathcal{I}$ is defined as

$$\mu_{\mathcal{I}}(\mathbf{A}) \triangleq \max_{i,j \in \mathcal{I}, i \neq j} \frac{|\langle \mathbf{A}_i, \mathbf{A}_j \rangle|}{\|\mathbf{A}_i\|_2 \|\mathbf{A}_j\|_2}, \tag{38}$$

where $\mathcal{I} \subseteq \{1, 2, \ldots, L\}$.

Let $\mathcal{I} = \hat{\mathcal{S}}_{\text{Last}}$. We propose minimizing the restricted mutual coherence $\mu_{\mathcal{I}}(\mathbf{A})$ to reduce computational complexity and to improve spectrum recovery performance in consecutive cognition cycles. We hereby extend the MC-RS algorithm to the RMC-RS algorithm, as detailed in Algorithm 4.

Compared with $\mu(\mathbf{A})$, $\mu_{\mathcal{I}}(\mathbf{A})$ is more decisive for successful spectrum recovery when $|\mathcal{I} \cap \mathcal{S}| \to |\mathcal{S}|$ and $|\mathcal{I}/\mathcal{S}| \to 0$. Moreover, in RMC-RS, an iteration number $m \sim 2^{|\mathcal{I}|}$ is sufficient. Since $|\mathcal{I}| < R$ usually holds, we have $2^{|\mathcal{I}|} \ll 2^R$, which significantly reduces the time complexity compared to MC-RS.

TABLE II
SUMMARY OF SIMULATION PARAMETERS

| Parameter | Value |
|---|---|
| Sensing bandwidth $B$ | 6000 MHz |
| # subbands $L$ | 40, 60, 80, 120 |
| # OFDM subcarriers $N_c$ | 52 |
| SNR | -10 $\sim$ 30 dB |
| OFDM channel bandwidth | 50 MHz |
| # active channels $k$ | 1 $\sim$ 8 |
| ADC sampling rate $f_s$ | 50 MSps |
| # cosets $R$ | 6$\sim$12 |
| # samples per frame $N$ | 24 |

## V. NUMERICAL EXPERIMENTS

The purpose of the experiments is to evaluate the performance of the proposed algorithms in comparison with uniform random sampling patterns and state-of-the-art (SOTA) algorithms for multicoset sampling pattern design, using synthetically generated realistic wireless signals with noise. All simulations were conducted in MATLAB 2022b running on an Intel Core i5-10310U processor.

### A. Simulation Setup

To model the wireless spectrum, we divide the frequency range $[0, B]$ evenly into $L$ subbands. We generate $k$ transmissions located on $k$ different subbands, whose indices are chosen randomly from the set $\{1, \ldots, L\}$ of size $k$. Each transmission is with exact bandwidth $B/L$ and consists of $N_c$ orthogonal frequency-division multiplexing (OFDM) subcarriers modulated with random quadrature phase shift keying (QPSK) symbols. To simulate real-world conditions, we introduce additive Gaussian noise across all subbands. On the receiver side, the received signal is first downconverted to the zero intermediate band $[-B/2, B/2]$, and demodulated into the in-phase (I) and quadrature (Q) components. A multicoset sampler samples the signal in $R$ cosets, with each coset equipped with a dual-channel ADC simutaneously sampling a copy of the I/Q pair.

We mainly focus on high-frequency bands, e.g., millimeter wave, where the traditional Nyquist sampling struggles to efficiently handle the extensive bandwidth in these high-frequency areas, thereby making CSS a preferable approach for these scenarios. Typically, the spectrum of interest spans from approximately 1 to 10 GHz. Given the constraints imposed by the sampling rate of commonly used low-power commercial ADCs, which typically hover around 10 to 250 MSps, practical parameters need to be set for optimal performance of CSS.

In our simulations, a typical value of $L$ is set between 40 and 160. Considering hardware complexity and effective spectrum sensing, $R$ is capped at 16. This cap is necessary for precisely detecting the OFDM channels within these high-frequency bands, with individual channel bandwidths ranging from around 50 to 400 MHz, as seen in the 5 G new radio (NR) standards. The defined simulation parameters are detailed in Table II.

Sampling patterns are generated using the proposed FFDG, MC-RS, and MC-SFS algorithms. For comparative analysis, patterns are also generated employing SOTA methods: the *Condition number Minimization* (Cond-Min) [5], *Condition number plus-L-minus-R Selection* (Cond-LRS) [10], and *Full-Kruskal-Rank Generation* (FKRG) algorithms [11]. Additionally, as a benchmark, uniform random sampling patterns are produced by randomly selecting $R$ delay factors from the set $\{1, \ldots, L\}$.

We construct the sensing matrix $\mathbf{A}$ according to (6). For the reconstruction of the spectrum support, the SOMP algorithm is employed. The SOMP is configured to cease operation upon concluding its $k$th iteration. The detection probability is then calculated using the expression $|\hat{\mathcal{S}} \cap \mathcal{S}|/|\mathcal{S}|$, where this ratio represents the intersection of the estimated and actual support sets relative to the size of the actual support set, thereby offering a precise evaluation of the detection capabilities within our established framework.

### B. Performance Evaluation of FFDG, MC-RS, and MC-SFS

Fig. 5(a) illustrates the relationship between detection probability and various signal sparsity levels $k$. For a valid comparison and compatibility with the restrictions of the FFDG algorithm, values $L$ and $R$ are defined as $L = 120 = 11^2 - 1$ and $R = 11$ as per (31)–(32) and (33). The generated signal, with an SNR of 20 dB, has a sparsity level chosen in the set $k \in \{1, 2, \ldots, 8\}$. For each sparsity level, a thousand simulation iterations per algorithm are conducted, and the results are subsequently averaged. In each instance, transmissions are generated within random subbands. The results underscore FFDG's superior performance for $k \leq 7$, attaining nearly $99\%$ accuracy, a notable distinction as other algorithms barely reach $90\%$. MC-SFS and MC-RS show as subsequent high performers, with MC-SFS slightly leading. All three proposed algorithms remarkably outperform Cond-Min and Cond-LRS algorithms, which only modestly outperform uniform selection. The FKRG algorithm significantly lags, exhibiting performance even below uniform selection due to its inherent deficiencies. Fig. 5(b) showcases similar results under $L = 40$ and $R = 8$, a scenario where FFDG is inapplicable.

Fig. 6(a) showcases the result of detection probability plotted against the SNR, spanning from $-10$ to 30 dB. In this scenario, the signal sparsity is maintained at $k = 4$. The other parameters remain unchanged. A similar trend in results is observed with varying sparsity levels. The FFDG algorithm continues to lead in performance, especially at higher SNR values, showing its robustness and adaptability in diverse SNR conditions. MC-RS and MC-SFS show commendable performance. Fig. 5(b) showcases the results given signal sparsity level $k = 3$, under $L = 40$ and $R = 8$, a scenario where FFDG is inapplicable,

A statistical analysis is conducted on the mutual coherence $\mu(\mathbf{A})$ of the sensing matrix resulting from the proposed algorithms. The results are shown in Fig. 7. With fixed $L = 120$ and $R$ varying from 7 to 12, the superiority of the proposed algorithms FFDG, MC-RS, and MC-SFS in our article becomes further emphasized. The $\mu(\mathbf{A})$ yielded by uniform selection remains at a significantly high level with large variance, underscoring its unreliability and inconsistency. Conversely, the MC-RS algorithm delivers a remarkably smaller $\mu(\mathbf{A})$ with a narrow confidence interval. Moreover, the MC-SFS algorithm guarantees a sampling pattern with a deterministic $\mu(\mathbf{A})$. The FFDG, despite a larger variation compared to MC-RS, assures

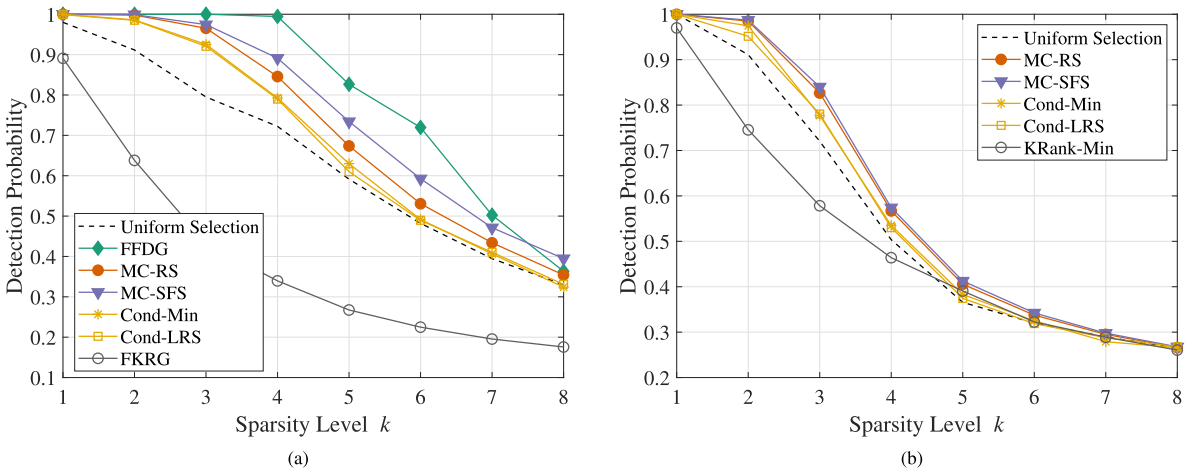


Fig. 5. Detection probability against signal sparsity level $k$. Simulations conducted with $k = 1 \sim 8$ averaged over 1000 runs under parameters (a) $R = 11, L = 120$, (b) $R = 8, L = 40$.

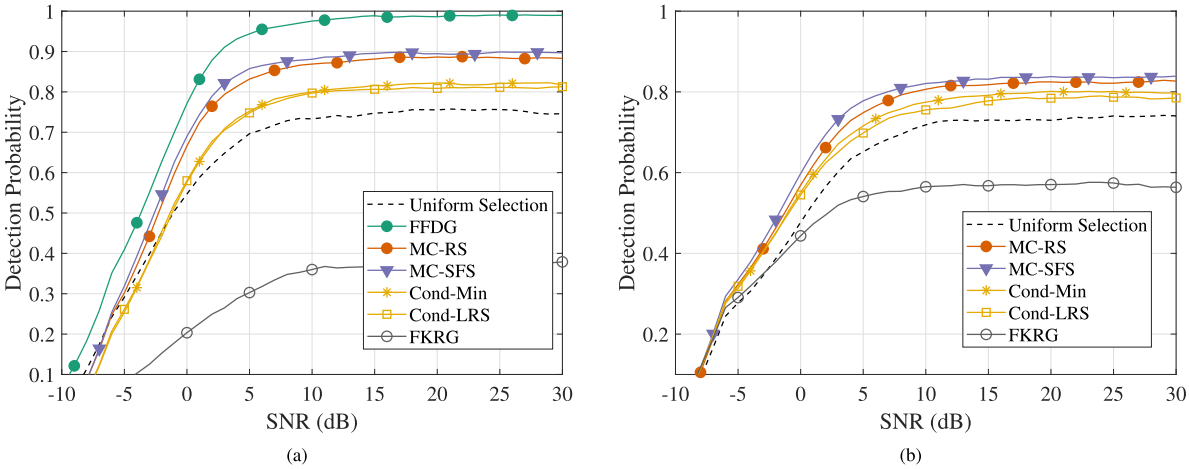


Fig. 6. Detection probability against SNR $= -10 \sim 30$ dB, with fixed signal sparsity, averaged over 1000 runs, conducted under parameters (a) $k = 4$, $R = 11$, $L = 120$, (b) $k = 3$, $R = 8$, $L = 40$.

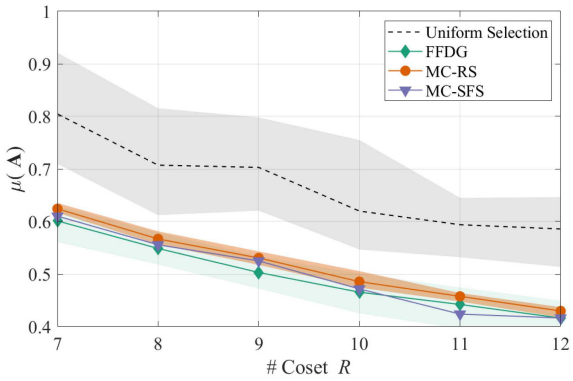


Fig. 7. Mutual coherence $\mu(\mathbf{A})$ against $R$ for $L = 120$ and $R = 7 \sim 12$. The figure showcases $\mu(\mathbf{A})$ values with a 95% confidence interval plotted in shade.

lower mean values of $\mu(\mathbf{A})$. The narrow confidence intervals and lower mean values associated with our proposed algorithms affirm their robustness and reliability.

### C. Performance Evaluation of RMC-RS

To simulate a change in the spectrum support, we applied two different spectrum supports for the initial 250 cognition cycles and the last 250. Both supports are randomly drawn from a uniform distribution across all subsets of $\{1, \ldots, 60\}$ with a cardinality of 6. In every cognition cycle, the signal is regenerated by modulating random QPSK symbols onto the OFDM subcarriers.

The RMC-RS algorithm was employed to generate sampling patterns over 500 consecutive cognition cycles, with parameters set at $R = 12$ and $L = 60$. In our simulation, the output of the RMC-RS in the first cognition cycle is a uniformly selected pattern. Subsequent outputs are computed based on the procedure described in Algorithm 4. For comparison, we also generated sampling patterns using uniform selection and the MC-RS algorithm for each cognition cycle.

After repeating the experiment 100 times, the average detection probability was computed for each cycle, shown in Fig. 8(a). The results revealed that the uniformly selected pattern led to

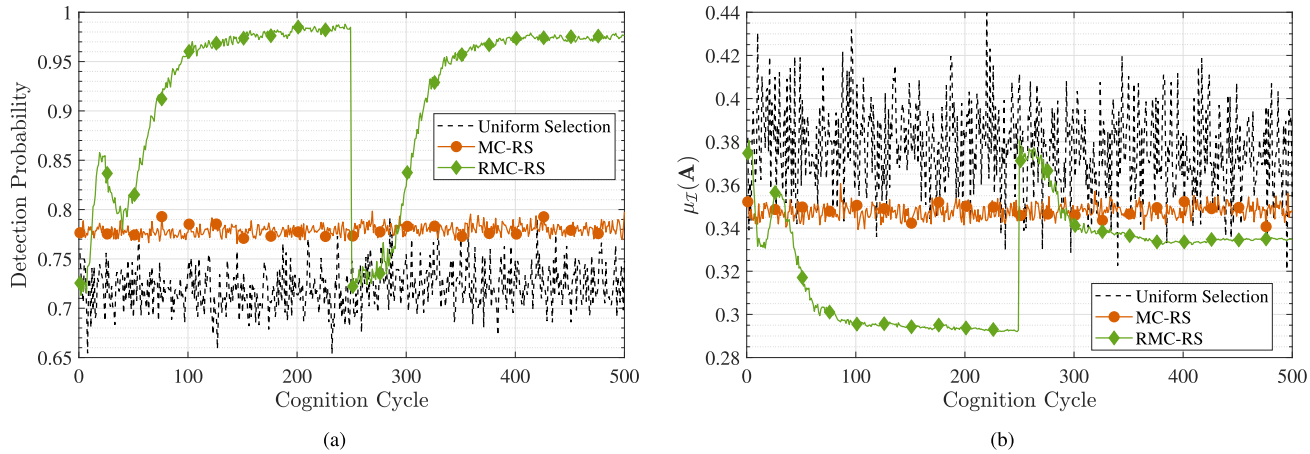


(a) (b)

Fig. 8. (a) Detection probability and (b) restricted mutual coherence $\mu_{\mathcal{I}}(\mathbf{A})$ (with $\mathcal{I} = \mathcal{S}$) over 500 consecutive cognition cycles using the RMC-RS algorithm iteratively in each cycle, with parameters $L = 60$, $R = 12$, and spectrum sparsity level $k = 6$. Results are compared with patterns generated by uniform selection and MC-RS.

fluctuating detection probabilities over time. In contrast, the sampling patterns generated by MC-RS maintained almost consistent detection probabilities across consecutive cognition cycles and generally outperformed the uniform selection method. The detection probability using RMC-RS starts at a level comparable to the uniformly selected pattern, then rapidly increases, settling at a value above 95% within approximately 100 cognition cycles. A noticeable drop in the detection probability of RMC-RS is observed at the 251st cognition cycle due to a significant shift in the spectrum support. However, it quickly reconverges, again reaching over 95% within the subsequent 100 cycles. The advantage of using RMC-RS is further reflected in the variations in the restricted mutual coherence over cognition cycles, illustrated in Fig. 8(b). With $\mathcal{I} = \mathcal{S}$ set, it becomes evident that $\mu_{\mathcal{I}}(\mathbf{A})$ related to RMC-RS swiftly converges to a minimal value when the spectrum support remains consistent. In comparison, the values corresponding to both uniform selection and MC-RS remain at the same level as the cognition cycles progress.

In Fig. 9, we illustrate the relationship between the percentage change in spectrum support and the consequent dip in detection probability. By manipulating the percentage ratio of change in spectrum support at the 250th cognition cycle, we observe variations in both the magnitude of the detection probability's decline and its subsequent re-convergence rate. Notably, with minimal changes to the spectrum support, the decrease in detection probability is modest, and re-convergence is swift. Conversely, as the percentage of the spectrum support change increases, there is a notable drop in detection probability followed by a slower re-convergence. It is crucial to highlight that, in real-world scenarios, transmissions are highly independent. Thus, the spectrum support is unlikely to undergo abrupt, significant alterations. Under such conditions, the RMC-RS consistently delivers robust performance, being capable of maintaining a high detection probability throughout long time periods.

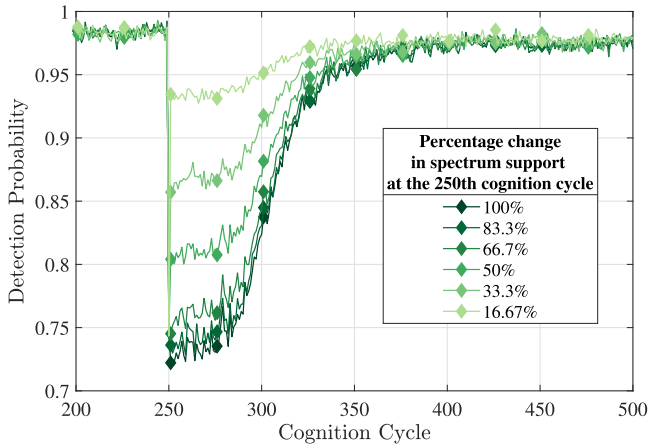


Fig. 9. Performance evaluation of the RMC-RS algorithm with $L = 60$, $R = 12$, and spectrum sparsity level $k = 6$. The graph illustrates the trend in detection probability from the 200th to the 500th cognition cycle. Notably, a decline in detection probability is observed at the 250th cycle due to varying percentage changes in spectrum support. This is followed by their respective re-convergence trajectories in the ensuing cycles.

TABLE III
TIME COMPLEXITY OF FFDG, MC-RS, MC-SFS, AND RMC-RS

| Algorithm | Time Complexity |
|---|---|
| FFDG | $O(R^3)$ |
| MC-RS | $O(2^R L^2 R)$ |
| MC-SFS | $O(L^3 R^2)$ |
| RMC-RS | $O(2^{\lvert\mathcal{I}\rvert} \lvert\mathcal{I}\rvert^2 R)$ |

### D. Time Complexity and Execution Time

The time complexities of the algorithms proposed are presented in Table III.

The time complexity of the FFDG algorithm is non-trivial. The nature of finite fields and the algorithms employed to deduce irreducible polynomials, primitive roots, and logarithms inherently influence the time complexity. While there are various

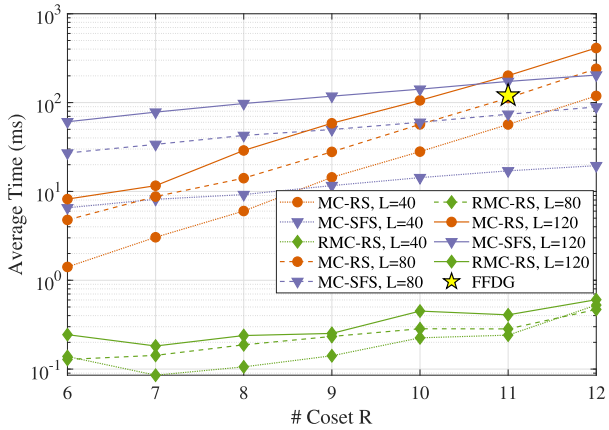


Fig. 10. Comparison of average running times for the FFDG, MC-RS, MC-SFS, and RMC-RS algorithms with parameters $L \in \{40, 80, 120\}$ and $R$ ranging from 6 to 12, plotted in logarithmic scale. For RMC-RS, we take $|\mathcal{I}| = \lfloor R/2 \rfloor$.

advanced methods to address the finite fields problems, for simplicity and clarity in this article, we have chosen to use the most naive approaches for its operations. The pivotal operations in Algorithm 1, evaluated using the most elementary (exhaustive search) algorithms, are:

- *Step 1:* Constructing $\mathbb{F}_R$ is a constant-time operation, represented as $O(1)$.
- *Step 2:* Identifying an irreducible polynomial in $\mathbb{F}_R[x]$ using a naive approach takes $O(R^3)$, due to polynomial irreducibility testing.
- *Step 3:* Constructing $\mathbb{F}_{R^n}$ takes $O(R)$.
- *Step 4:* Finding a primitive root in a finite field using a naive method takes $O(R^2)$, as each root candidate's powers must be validated.
- *Step 5:* With rudimentary methods, computing logarithms for each field element takes $O(R^2)$, considering the need to verify up to $R$ base powers for each element.

The dominant time complexity is $O(R^3)$, primarily driven by the irreducible polynomial search.

Fig. 10 shows the real-world execution times. The MC-RS algorithm, with a complexity of $O(2^R L^2 R)$, shows efficiency especially when $R$ is small. As $R$ increases, the $2^R$ factor in MC-RS leads to exponential growth in execution time. With larger $R$, MC-SFS outperforms MC-RS in time efficiency. In practice, the selection between MC-SFS and MC-RS should reflect the unique application needs and specific values of $L$ and $R$.

For RMC-RS, considering $\mathcal{I} = \hat{\mathcal{S}}_{\text{Last}}$, we ensure $|\mathcal{I}| \leq R < L$. In a sparsely occupied wideband spectrum, $|\mathcal{I}|$ is much less than $L$. Given RMC-RS's focus on atoms indexed by $\mathcal{I}$, leading to $m \approx 2^{|\mathcal{I}|}$, it significantly reduces computational costs relative to MC-RS, making RMC-RS a preferable choice for multicoset sensing matrix design in consecutive cognition cycles.

The proposed algorithms have been implemented on a self-developed hardware platform and have provided high-quality sub-Nyquist datasets for a series of signal processing and learning competitions named *GHz Bandwidth Sensing* (*GBSense*) challenges, which were successfully held in 2021 and 2022 [47].

## VI. Conclusion

In this article, we investigated the design of sampling patterns for multicoset samplers in a noisy setup. The proposed algorithms guarantee successful spectrum recovery for compressed spectrum sensing in a practical environment with noise, thereby facilitating the dynamic spectrum access of low-power mobile cognitive radio devices.

Our main contributions lie in efficient sampling pattern design algorithms to yield mutually incoherent sensing matrices. First, we generate a partial inverse Fourier matrix in a deterministic manner by constructing a finite field. The matrix is proved to have a strict upper bound of mutual coherence. Then we proposed the FFDG algorithm to generate sampling patterns that satisfy the above upper bound. The FFDG algorithm provides faithful spectrum reconstruction performance but imposes some mild restrictions on the coset number and the downsampling factor of the multicoset sampler.

We then proposed two optimization methods to design sampling patterns without any restrictions on the coset number and the downsampling factor of the multicoset sampler. The MC-RS algorithm employs a random search strategy and can find a nearly optimal sampling pattern within far fewer iterations than conventional exhaustive search methods. The choice of the iteration number is investigated by analyzing the distribution of mutual coherence under certain coset numbers and downsampling factors. The MC-RS algorithm is efficient when the coset number is relatively small, and its iteration number increases exponentially as the coset number increases linearly. The MC-SFS algorithm provides high computational efficiency for relatively large coset numbers. It minimizes the mutual coherence of the sensing matrix using a greedy pursuit strategy. It can find a sampling pattern whose corresponding mutual coherence is locally optimal.

In addition, we proposed the RMC-RS algorithm for the scenario that requires dynamic sampling patterns to provide better robustness. The algorithm adjusts the sampling pattern between consecutive cognition cycles by minimizing a restricted version of the mutual coherence of the sensing matrix. The RMC-RS algorithm shows extremely low time complexity and strong adaptability to the genuine support of the spectrum.

Numerical experiments demonstrated outstanding spectrum recovery performance of the proposed algorithms using simulated OFDM signals with noise. The feasibility of the proposed algorithm is also proved on a self-developed hardware platform by providing high-quality sub-Nyquist datasets for a series of influential competitions held in 2021 and 2022.

## References

[1] Q. Zhao and B. M. Sadler, "A survey of dynamic spectrum access," *IEEE Signal Process. Mag.*, vol. 24, no. 3, pp. 79–89, May 2007.

[2] Z. Song, Y. Gao, and R. Tafazolli, "A survey on spectrum sensing and learning technologies for 6G," *IEICE Trans. Commun.*, vol. 104-B, 2021, Art. no. 2020DSI0002.

[3] R. Venkataramani and Y. Bresler, "Optimal sub-nyquist nonuniform sampling and reconstruction for multiband signals," *IEEE Trans. Signal Process.*, vol. 49, no. 10, pp. 2301–2313, Oct. 2001.
[4] T. Moon, H. W. Choi, N. Tzou, and A. Chatterjee, "Wideband sparse signal acquisition with dual-rate time-interleaved undersampling hardware and multicoset signal reconstruction algorithms," *IEEE Trans. Signal Process.*, vol. 63, no. 24, pp. 6486–6497, Dec. 2015.
[5] D. D. Arianandа and G. Leus, "Compressive wideband power spectrum estimation," *IEEE Trans. Signal Process.*, vol. 60, no. 9, pp. 4775–4789, Sep. 2012.
[6] C.-P. Yen, Y. Tsai, and X. Wang, "Wideband spectrum sensing based on sub-Nyquist sampling," *IEEE Trans. Signal Process.*, vol. 61, no. 12, pp. 3028–3040, Jun. 2013.
[7] M. Mishali and Y. C. Eldar, "Blind multiband signal reconstruction: Compressed sensing for analog signals," *IEEE Trans. Signal Process.*, vol. 57, no. 3, pp. 993–1009, Mar. 2009.
[8] D. L. Donoho and M. Elad, "Optimally sparse representation in general (nonorthogonal) dictionaries via l1 minimization," *Proc. Nat. Acad. Sci.*, vol. 100, no. 5, pp. 2197–2202, 2003.
[9] P. Feng and Y. Bresler, "Spectrum-blind minimum-rate sampling and reconstruction of multiband signals," in *Proc. IEEE Int. Conf. Acoustics, Speech, Signal Process. Conf. Proc.*, 1996, pp. 1688–1691.
[10] H. B. Celebi, L. Durak-Ata, and H. Celebi, "Multi-coset sampling and reconstruction of signals: Exploiting sparsity in spectrum monitoring," in *Proc. 21st Eur. Signal Process. Conf.*, 2013, pp. 1–5.
[11] M.-E. Domínguez-Jiménez, N. González-Prelcic, G. Vazquez-Vilar, and R. López-Valcarce, "Design of universal multicoset sampling patterns for compressed sensing of multiband sparse signals," in *Proc. IEEE Int. Conf. Acoust., Speech Signal Process.*, 2012, pp. 3337–3340.
[12] B. Tausiesakul and N. Gonz ález-Prelcic, "Power spectrum blind sampling using optimal multicoset sampling patterns in the MSE sense," in *Proc. IEEE Int. Conf. Acoust., Speech Signal Process.*, 2014, pp. 1055–1059.
[13] E. J. Candes and T. Tao, "Decoding by linear programming," *IEEE Trans. Inf. Theory*, vol. 51, no. 12, pp. 4203–4215, Dec. 2005.
[14] D. L. Donoho et al., "Uncertainty principles and ideal atomic decomposition," *IEEE Trans. Inf. Theory*, vol. 47, no. 7, pp. 2845–2862, Nov. 2001.
[15] R. A. DeVore, "Deterministic constructions of compressed sensing matrices," *J. Complexity*, vol. 23, no. 4/6, pp. 918–925, 2007.
[16] L. Welch, "Lower bounds on the maximum cross correlation of signals (corresp)," *IEEE Trans. Inf. Theory*, vol. 20, no. 3, pp. 397–399, May 1974.
[17] T. Strohmer and R. W. Heath Jr, "Grassmannian frames with applications to coding and communication," *Appl. Comput. Harmon. Anal.*, vol. 14, no. 3, pp. 257–275, 2003.
[18] B. M. Hochwald, T. L. Marzetta, T. J. Richardson, W. Sweldens, and R. Urbanke, "Systematic design of unitary space-time constellations," *IEEE Trans. Inf. Theory*, vol. 46, no. 6, pp. 1962–1973, Sep. 2000.
[19] S. Satake and Y. Gu, "Constructions of complex codebooks asymptotically meeting the welch bound: A graph theoretic approach," in *Proc. IEEE Int. Symp. Inf. Theory*, 2020, pp. 48–53.
[20] P. Xia, S. Zhou, and G. B. Giannakis, "Achieving the welch bound with difference sets," *IEEE Trans. Inf. Theory*, vol. 51, no. 5, pp. 1900–1907, May 2005.
[21] D. V. Sarwate, "Meeting the welch bound with equality," in *Proc. Sequences Appl.*, 1999, pp. 79–102.
[22] Z. Song, J. Yang, H. Zhang, and Y. Gao, "Approaching sub-nyquist boundary: Optimized compressed spectrum sensing based on multicoset sampler for multiband signal," *IEEE Trans. Signal Process.*, vol. 70, pp. 4225–4238, 2022.
[23] N. M. Katz, "An estimate for character sums," *J. Amer. Math. Soc.*, vol. 2, no. 2, pp. 197–200, 1989.
[24] G. Xu and Z. Xu, "Compressed sensing matrices from fourier matrices," *IEEE Trans. Inf. Theory*, vol. 61, no. 1, pp. 469–478, Jan. 2015.
[25] J. A. Tropp, A. C. Gilbert, and M. J. Strauss, "Simultaneous sparse approximation via greedy pursuit," in *Proc. IEEE Int. Conf. Acoustics, Speech, Signal Process.*, 2005, pp. v/721–v/724.
[26] S. S. Chen, D. L. Donoho, and M. A. Saunders, "Atomic decomposition by basis pursuit," *SIAM Rev.*, vol. 43, no. 1, pp. 129–159, 2001.
[27] D. L. Donoho and M. Elad, "On the stability of the basis pursuit in the presence of noise," *Signal Process.*, vol. 86, no. 3, pp. 511–532, 2006.
[28] R. Tibshirani, "Regression shrinkage and selection via the lasso," *J. Roy. Stat. Soc.: Ser. B. (Methodological)*, vol. 58, no. 1, pp. 267–288, 1996.
[29] S. A. Van De Geer and P. Bühlmann, "On the conditions used to prove oracle results for the lasso," *Electron. J. Statist.*, vol. 3, pp. 1360–1392, 2009.
[30] Y. She, J. Shen, and A. Barbu, "Slow-kill for Big Data learning," *IEEE Trans. Inf. Theory*, vol. 69, no. 9, pp. 5936–5955, Sep. 2023.
[31] Y. She, H. Li, J. Wang, and D. Wu, "Grouped iterative spectrum thresholding for super-resolution sparse spectrum selection," *IEEE Trans. Signal Process.*, vol. 61, no. 24, pp. 6371–6386, Dec. 2013.
[32] H. Li, L. Wang, X. Zhan, and D. K. Jain, "On the fundamental limit of orthogonal matching pursuit for multiple measurement vector," *IEEE Access*, vol. 7, pp. 48860–48866, 2019.
[33] J.-F. Determe, J. Louveaux, L. Jacques, and F. Horlin, "On the exact recovery condition of simultaneous orthogonal matching pursuit," *IEEE Signal Process. Lett.*, vol. 23, no. 1, pp. 164–168, Jan. 2016.
[34] X. Yang, A. Liao, and J. Xie, "A remark on joint sparse recovery with OMP algorithm under restricted isometry property," *Appl. Math. Comput.*, vol. 316, pp. 18–24, 2018.
[35] T. T. Cai, G. Xu, and J. Zhang, "On recovery of sparse signals via -minimization," *IEEE Trans. Inf. Theory*, vol. 55, no. 7, pp. 3388–3397, Jul. 2009.
[36] M. Rudelson and R. Vershynin, "On sparse reconstruction from fourier and gaussian measurements," *Commun. Pure Appl. Math.*, vol. 61, no. 8, pp. 1025–1045, 2010.
[37] Y. C. Eldar and M. Mishali, "Robust recovery of signals from a structured union of subspaces," *IEEE Trans. Inf. Theory*, vol. 55, no. 11, pp. 5302–5316, Nov. 2009.
[38] Y. C. Eldar, P. Kuppinger, and H. Bolcskei, "Block-sparse signals: Uncertainty relations and efficient recovery," *IEEE Trans. Signal Process.*, vol. 58, no. 6, pp. 3042–3054, Jun. 2010.
[39] Y. Zhao and Z. Luo, "Improved rip-based bounds for guaranteed performance of two compressed sensing algorithms," *Sci. China Math.*, vol. 66, no. 5, pp. 1123–1140, 2023.
[40] X. Yuan, P. Li, and T. Zhang, "Exact recovery of hard thresholding pursuit," in *Proc. Adv. Neural Inf. Process. Syst.*, 2016, pp. 3565–3573.
[41] Y. She, J. Shen, and A. Barbu, "Slow kill for Big Data learning," *IEEE Trans. Inf. Theory*, vol. 69, no. 9, pp. 5936–5955, Sep. 2023.
[42] J. A. Tropp, A. C. Gilbert, and M. J. Strauss, "Algorithms for simultaneous sparse approximation. part I: Greedy pursuit," *Signal Process.*, vol. 86, no. 3, pp. 572–588, 2006.
[43] I. Shparlinski, "On finding primitive roots in finite fields," *Theor. Comput. Sci.*, vol. 157, no. 2, pp. 273–275, 1996.
[44] D. Shanks, "Class number, a theory of factorization, and genera," in *Proc. Symp. Math. Soc.*, 1971, pp. 41–440.
[45] L. Rastrigin, "The convergence of the random search method in the extremal control of a many parameter system," *Automat. Remote Control*, vol. 24, pp. 1337–1342, 1963.
[46] J. Mitola and G. Q. Maguire, "Cognitive radio: Making software radios more personal," *IEEE Pers. Commun.*, vol. 6, no. 4, pp. 13–18, Aug. 1999.
[47] Y. Gao et al., "Sub-Nyquist spectrum sensing and learning challenge," *Front. Comput. Sci.*, vol. 15, no. 4, pp. 1–5, 2021.

**Zihang Song** (Member, IEEE) received the BS and MS degrees from Beihang University, China, and the PhD degree in information and communication systems from the University of Surrey, U.K., in 2023. He is currently a research associate with King's College London, U.K. His research interests include sparse signal processing, physical layer design for wireless communication systems, low-power AI computing platforms for 5G/6G, in-memory computing, and neuromorphic computing. He is involved with the King's Communication, Learning & Information Processing Lab and King's Laboratory for Intelligent Computing.

**Yiyuan She** (Senior Member, IEEE) received the PhD degree in statistics from Stanford University, in 2008. He is a professor with the Department of Statistics, Florida State University, Tallahassee, FL, US. His research interests are in the areas of high dimensional statistics, statistical machine learning, optimization, signal processing, robust statistics, multivariate statistics, and network science. He received Florida State University Developing Scholar Award and the NSF CAREER award. He has served as an associate editor for *IEEE Transactions on Network Science and Engineering*, *Statistica Sinika*, and *Journal of the American Statistical Association*. He is fellow of ASA, fellow of IMS, and an elected member of ISI.

**Jian Yang** (Member, IEEE) received the BS degree in electronic information engineering (Underwater Acoustics) from the Harbin Engineering University, in 2015, and the PhD degree in information and communication engineering from the Harbin Institute of Technology, in 2022. From 2020 to 2021, he was a PhD visiting student with the School of Electronic Engineering and Computer Science, Queen Mary University of London. Since 2022, he has been an engineer with the China Academy of Information and Communications Technology (CAICT). His research interests focus on B5G/6G, cognitive radio, compressed sensing, and sub-Nyquist signal processing.

**Jinbo Peng** (Student Member, IEEE) received the BS degree in physics from Fudan University, Shanghai, China, in 2022. He is currently working toward the PhD degree with the Department of Computer Science and Technology, Fudan University. His research interests include 6G, satellite communication, compressed sensing and sub-Nyquist signal processing.

**Yue Gao** (Fellow, IEEE) received the PhD from the Queen Mary University of London (QMUL), U.K., in 2007. He is a chair professor with the School of Computer Science, director with the Intelligent Networking and Computing Research Centre, Fudan University, China and a visiting professor with the University of Surrey, U.K. He has worked as a lecturer, senior lecturer, reader and chair professor with QMUL and the University of Surrey, respectively. His research interests include smart antennas, sparse signal processing and cognitive networks for mobile and satellite systems. He has published more than 200 peer-reviewed journal and conference papers and more than 7000 citations. He was a co-recipient of the EU Horizon Prize Award on Collaborative Spectrum Sharing in 2016 and elected an Engineering and Physical Sciences Research Council fellow, in 2017. He is a member of the Board of Governors and distinguished lecturer of the IEEE Vehicular Technology Society (VTS), chair of the IEEE ComSoc Wireless Communication Technical Committee, and past chair of the IEEE ComSoc Technical Committee on Cognitive Networks. He has been an editor of several IEEE Transactions and Journals, and Symposia chair, Track chair, and other roles in the organizing committee of several IEEE ComSoC, VTS, and other conferences.

**Rahim Tafazolli** (Senior Member, IEEE) is currently a professor and the director of ICS and 5GIC, University of Surrey. He has more than 30 years of experience in digital communications research and teaching. He also heads one of Europa's leading research groups. He is regularly invited by governments to advise on the network and 5G technologies and was an advisor to the Mayor of London with regard to the London Infrastructure Investment 2050 Plan during May and June 2014. He has authored or co-authored more than 500 research papers in refereed journals, international conferences, and as an invited speaker. He is the editor of two books on "Technologies for Wireless Future" published by (Wiley Vol.1 in 2004 and Vol.2 2006). He is co-inventor on more than 30 granted patents, all in the field of digital communications. He was appointed fellow of WWRF (Wireless World Research Forum), in April 2011, in recognition of his personal contribution to the wireless world.